Leptonic or Hadronic Emission: The X-Ray Radiation Mechanism of Large-scale Jet Knots in 3C 273

Zhen-Jie Wang[1], Jin Zhang[2], Xiao-Na Sun[3], and En-Wei Liang[1]

[1] Guangxi Key Laboratory for Relativistic Astrophysics, School of Physical Science and Technology, Guangxi University, Nanning 530004, People's Republic of China

[2] Key Laboratory of Space Astronomy and Technology, National Astronomical Observatories, Chinese Academy of Sciences, Beijing 100012, People's Republic of China; jinzhang@bao.ac.cn

[3] School of Astronomy and Space Science, Nanjing University, Nanjing 210093, People's Republic of China

Abstract

A comprehensively theoretical analysis of the broadband spectral energy distributions (SEDs) of large-scale jet knots in 3C 273 is presented to reveal their X-ray radiation mechanism. We show that these SEDs cannot be explained with a single-electron population model when the Doppler boosting effect is either considered or not. By adding a more energetic electron (the leptonic model) or proton (the hadronic model) population, the SEDs of all knots are well represented. In the leptonic model, the electron population that contributes the X-ray emission is more energetic than the one responsible for the radio-optical emission by almost two orders of magnitude; the derived equipartition magnetic field strengths (B_{eq}) are ~0.1 mG. In the hadronic model, protons with energy ~20 PeV are required to interpret the observed X-rays; the B_{eq} values are several mG, larger than those in the leptonic model. Based on the fact that no resolved substructures are observed in these knots and the fast cooling time of the high-energy electrons does not easily explain the observed X-ray morphologies, we argue that the two distinct electron populations accelerated in these knots are unreasonable and their X-ray emission is attributed to the proton synchrotron radiation accelerated in these knots. In cases where these knots have relativistic motion toward the observer, the super-Eddington issue of the hadronic model can be avoided. Multiwavelength polarimetry and γ-ray observations with high resolution may be helpful to discriminate these models.

Unified Astronomy Thesaurus concepts: Galaxy jets (601); Active galactic nuclei (16); Non-thermal radiation sources (1119); X-ray active galactic nuclei (2035)

1. Introduction

The jets of some active galactic nuclei (AGNs) can extend to kiloparsec through megaparsec scales. The substructures of these large-scale jets have been resolved in the radio, optical, and X-ray bands and are defined as knots, hotspots, and lobes (Harris & Krawczynski 2006, and references therein). The radio-optical radiation of the substructures in large-scale jets is believed to be produced by the synchrotron process of relativistic electrons on account of the polarimetry; however, the X-ray emission mechanism has been a debated issue since the detection of X-ray radiation in these substructures (Harris & Krawczynski 2006, and references therein). The consistency between the X-ray spectrum and the extrapolation of the radio-optical synchrotron emission indicates the same synchrotron radiation origin of X-ray emission (Sambruna et al. 2007; Zhang et al. 2010, 2018a). But for most substructures, the hard spectra in the X-ray band require a new radiation component that is different from the low-energy band, and the inverse Compton (IC) scattering process has been suggested to explain the X-ray emission (e.g., Kataoka & Stawarz 2005; Zhang et al. 2010, 2018a), i.e., the synchrotron-self-Compton (SSC, Stawarz et al. 2007) model and the IC scattering of the cosmic microwave background (IC/CMB, Georganopoulos & Kazanas 2003; Abdo et al. 2010; McKeough et al. 2016; Wu et al. 2017; Guo et al. 2018; Zhang et al. 2018b) model. The X-ray emission may be produced by the synchrotron radiation of the second electron population that is different from the radio-optical emission (e.g., Zhang et al. 2009; Zargaryan et al. 2017; Sun et al. 2018). It can also be from the synchrotron radiation of

protons in the extended regions of large-scale jets (Aharonian 2002; Kundu & Gupta 2014).

3C 273 is a typical γ-ray emitting flat spectrum radio quasar located at $z = 0.158$ (Schmidt 1963). Its one-side knotty jet in the radio band extends to ~21″ from the nucleus, but its optical emission is observed only from 12″ outward (Jester et al. 2005; Uchiyama et al. 2006). The observed morphology at wavelengths from 3.6 cm to 300 nm is similar (Jester et al. 2005). Using ground-based imaging in the radio (Conway et al. 1993), near-infrared (Neumann et al. 1997), and optical bands (Meisenheimer et al. 1996; Röser et al. 2000), the radio–IR-optical continuua are obtained for the hotspot and the brightest knots, and they can be explained by the synchrotron radiation of a single power-law electron population (Jester et al. 2005). On the basis of the deep Very Large Array and Hubble Space Telescope (HST) observations of the large-scale jet, the excess near-ultraviolet over the radio-optical synchrotron radiation is revealed (Jester et al. 2005), thus a two-component model is necessary to describe the broadband spectral energy distributions (SEDs) of these substructures. This is further confirmed by the far-ultraviolet observations at ~150 nm with the HST; the far-ultraviolet fluxes of these substructures are compatible with the extrapolation of the X-ray power law down to the ultraviolet (UV) band (Jester et al. 2007). The optical polarization is consistent with the radio polarization in degree and orientation, indicating that the optical emission is likely of synchrotron origin, like the radio emission (Uchiyama et al. 2006). Zhang et al. (2018a) reported that the broadband SEDs from the radio to X-ray bands of the large-scale jet knots in 3C 273 cannot be well represented by the radiation of a single-

Table 1
Parameters in Scenario I: A Single Electron Population

Knot	A_1 (1/eV)	E_b (GeV)	p_1	p_2	E_{total} (erg)	Γ	δ	B[a] (μG)	B_{eq} (μG)	$\log P_e$ (erg s^{-1})	R (arcsec)
$\delta = 1$											
A	$3.1^{+0.5}_{-0.4}$E45	1230^{+70}_{-170}	$2.47^{+0.02}_{-0.02}$	$5.0^{+0.4}_{-0.4}$	$6.9^{+0.6}_{-0.6}$E60	1	1	$0.65^{+0.03}_{-0.03}$	11600^{+500}_{-500}	49.36	0.8
B1	$2.5^{+0.3}_{-0.3}$E44	900^{+90}_{-90}	$2.59^{+0.01}_{-0.01}$	$5.6^{+0.5}_{-0.5}$	$2.4^{+0.1}_{-0.2}$E60	1	1	$1.8^{+0.1}_{-0.1}$	10500^{+200}_{-200}	49.02	0.6
B2	$3.5^{+1.3}_{-0.6}$E45	490^{+60}_{-40}	$2.28^{+0.03}_{-0.04}$	$3.76^{+0.09}_{-0.06}$	$9.9^{+1.1}_{-1.1}$E59	1	1	$1.0^{+0.1}_{-0.1}$	4400^{+200}_{-200}	48.52	0.8
B3	$2.3^{+0.9}_{-0.5}$E45	510^{+200}_{-50}	$2.10^{+0.03}_{-0.05}$	$3.93^{+0.40}_{-0.11}$	$1.1^{+0.1}_{-0.1}$E59	1	1	$1.1^{+0.1}_{-0.1}$	2290^{+60}_{-80}	47.70	0.6
C1	$5.8^{+1.1}_{-1.1}$E45	575^{+70}_{-15}	$1.90^{+0.02}_{-0.03}$	$4.51^{+0.09}_{-0.11}$	$6.6^{+1.1}_{-0.3}$E58	1	1	$1.5^{+0.1}_{-0.2}$	1740^{+150}_{-140}	47.47	0.6
C2	$7.2^{+0.7}_{-1.2}$E45	380^{+100}_{-40}	$1.89^{+0.02}_{-0.02}$	$4.25^{+0.30}_{-0.11}$	$7.4^{+1.5}_{-0.7}$E58	1	1	$2.1^{+0.2}_{-0.2}$	1470^{+140}_{-70}	47.45	0.7
D1	$9.9^{+1.5}_{-1.0}$E45	374^{+15}_{-15}	$1.76^{+0.02}_{-0.02}$	$4.73^{+0.06}_{-0.06}$	$5.5^{+0.3}_{-0.2}$E58	1	1	$2.8^{+0.1}_{-0.1}$	1260^{+40}_{-30}	47.32	0.7
D2H3	$1.7^{+0.3}_{-0.3}$E46	217^{+30}_{-9}	$1.72^{+0.03}_{-0.03}$	$4.49^{+0.19}_{-0.06}$	$7.0^{+0.7}_{-0.3}$E58	1	1	$4.4^{+0.2}_{-0.3}$	834^{+40}_{-17}	47.27	1.0
H2	$4.0^{+0.8}_{-0.5}$E43	25^{+8}_{-8}	$2.25^{+0.03}_{-0.03}$	$4.2^{+0.2}_{-0.2}$	$7.7^{+1.1}_{-1.1}$E57	1	1	$72.4^{+1.1}_{-1.1}$	470^{+30}_{-30}	46.47	0.7
$\delta > 1$											
A	$6.8^{+1.2}_{-0.8}$E38	112^{+19}_{-10}	$2.54^{+0.01}_{-0.02}$	$4.05^{+0.40}_{-0.17}$	$3.5^{+0.2}_{-0.2}$E54	$22.4^{+1.9}_{-1.9}$	$17^{+0.3}_{-0.4}$	$8.3^{+0.2}_{-0.2}$	$8.3^{+0.2}_{-0.2}$	45.77	0.8
B1	$4.5^{+0.4}_{-0.4}$E38	72^{+7}_{-7}	$2.53^{+0.01}_{-0.01}$	$3.99^{+0.11}_{-0.11}$	$2.1^{+0.1}_{-0.1}$E54	$12.6^{+0.3}_{-0.2}$	$16.6^{+0.1}_{-0.1}$	$9.8^{+0.2}_{-0.2}$	$9.8^{+0.2}_{-0.2}$	45.16	0.6
B2	$7.8^{+1.2}_{-0.8}$E38	81^{+9}_{-9}	$2.55^{+0.02}_{-0.02}$	$3.94^{+0.13}_{-0.13}$	$4.6^{+0.2}_{-0.2}$E54	$12.3^{+0.1}_{-0.1}$	$16.5^{+0.1}_{-0.1}$	$9.5^{+0.3}_{-0.3}$	$9.5^{+0.3}_{-0.3}$	45.36	0.8
B3	$1.3^{+0.3}_{-0.1}$E40	59^{+6}_{-6}	$2.08^{+0.01}_{-0.04}$	$3.91^{+0.12}_{-0.12}$	$4.6^{+0.5}_{-0.5}$E53	$13.6^{+1.3}_{-0.5}$	$16.9^{+0.3}_{-0.2}$	$4.6^{+0.1}_{-0.3}$	$4.6^{+0.1}_{-0.3}$	44.58	0.6
C1	$4.2^{+0.3}_{-0.2}$E39	104^{+1}_{-1}	$2.31^{+0.01}_{-0.01}$	$4.57^{+0.04}_{-0.01}$	$1.6^{+0.1}_{-0.1}$E54	$10.2^{+0.2}_{-0.1}$	$15.2^{+0.2}_{-0.1}$	$8.5^{+0.1}_{-0.3}$	$8.5^{+0.1}_{-0.3}$	44.85	0.6
C2	$3.2^{+0.4}_{-0.3}$E40	67^{+2}_{-5}	$2.12^{+0.01}_{-0.01}$	$4.24^{+0.04}_{-0.09}$	$1.6^{+0.1}_{-0.1}$E54	$10.6^{+0.4}_{-0.2}$	$15.5^{+0.3}_{-0.1}$	$6.9^{+0.2}_{-0.3}$	$6.9^{+0.2}_{-0.3}$	44.84	0.7
D1	$2.2^{+0.3}_{-0.2}$E40	86^{+2}_{-1}	$2.23^{+0.01}_{-0.02}$	$4.76^{+0.07}_{-0.14}$	$3.3^{+0.1}_{-0.1}$E54	$8.3^{+0.2}_{-0.2}$	$13.5^{+0.2}_{-0.2}$	$9.8^{+0.2}_{-0.3}$	$9.8^{+0.2}_{-0.3}$	44.94	0.7
D2H3	$2.1^{+0.2}_{-0.6}$E41	53^{+3}_{-6}	$2.09^{+0.02}_{-0.02}$	$4.34^{+0.06}_{-0.06}$	$8.2^{+0.5}_{-0.7}$E54	$7.2^{+0.2}_{-0.1}$	$12.3^{+0.3}_{-0.2}$	$9.0^{+0.3}_{-0.4}$	$9.0^{+0.3}_{-0.4}$	45.05	1.0
H2	$2.5^{+0.4}_{-0.3}$E41	16^{+7}_{-5}	$2.19^{+0.02}_{-0.03}$	$4.3^{+0.3}_{-0.2}$	$2.5^{+0.2}_{-0.4}$E55	$3.7^{+0.2}_{-0.1}$	$7.0^{+0.3}_{-0.2}$	$26.9^{+1.0}_{-2.0}$	$26.9^{+1.0}_{-2.0}$	45.12	0.7

Note.
[a] $B < B_{eq}$ in the $\delta = 1$ case and $B = B_{eq}$ in the $\delta > 1$ case; for more details see the text.

electron population, including synchrotron emission, and the SSC and IC/CMB processes.

In this paper, we use three different models to reproduce the SEDs in the radio–IR–optical–UV–X-ray bands of nine large-scale jet knots in 3C 273 to reveal their X-ray radiation mechanism. The SED data of the nine knots are taken from Jester et al. (2007). The SED modeling is given in Section 2. A discussion of the fitting results and a summary are presented in Sections 3 and 4, respectively. Throughout, $H_0 = 71 \ \mathrm{km \ s^{-1} \ Mpc^{-1}}$, $\Omega_m = 0.27$, and $\Omega_\Lambda = 0.73$ are adopted.

2. SED Modeling

The Doppler booting effect is critical in modeling the SEDs of jets. The Doppler factor (δ) of the relativistic jet at the parsec scale in 3C 273 has been estimated using flux-density variations[4] at the radio band (Hovatta et al. 2009; Liodakis et al. 2017) or broadband SED modeling (e.g., Zhang et al. 2014). It was also proposed that the jets would be seriously decelerated at the kiloparsec scale (e.g., Arshakian & Longair 2004; Uchiyama et al. 2006; Mullin & Hardcastle 2009; Meyer et al. 2016). Recently, using multi-epoch images observed by the HST over the past 20 years, Meyer et al. (2016) reported that the kiloparsec-scale knots in 3C 273 are compatible with being stationary, with a mean speed of $-0.2 \pm 0.5c$ over the whole jet. Due to the uncertainty of this issue, we model the SEDs in two cases: without considering the beaming effect ($\delta = 1$) and considering the beaming effect ($\delta > 1$). Note that

---

[4] Compared with the variability of the core radiation, the emission of substructures in large-scale jets almost does not show any variation, which is also used to estimate the origin of the γ-ray emission (e.g., Guo et al. 2018; Zhang et al. 2018b; Meyer et al. 2019).

$\delta = 1/[\Gamma - (\Gamma^2 - 1)^{1/2} \cos \theta]$, where θ is the viewing angle and Γ is the bulk Lorenz factor of the emission region. We take $\theta = 3°.3$ (Hovatta et al. 2009) for all the knots.

The synchrotron radiation, SSC, and IC/CMB processes of relativistic electrons (leptonic model) and protons (hadronic model) are the candidate radiation mechanisms in our analysis. The radiation region is assumed to be a sphere with radius R, which is derived from the angular radius and taken from Jester et al. (2005), as listed in Table 1. The CMB peak frequency at $z = 0$ is $\nu_{CMB} = 1.6 \times 10^{11}$ Hz and the CMB energy density in the comoving frame is $U'_{CMB} = \frac{4}{3} \Gamma^2 U_{CMB}(1 + z)^4$ (Dermer & Schlickeiser 1994; Georganopoulos et al. 2006), where $U_{CMB} = 4.2 \times 10^{-13}$ erg cm^{-3}. The number distributions of the electrons and/or protons are taken as an exponential cutoff power law or a broken power law.

1. Broken power law:

$$N_1(E) = A_1 \begin{cases} \left(\dfrac{E}{E_0}\right)^{-p_1} & E \leqslant E_b \\ \left(\dfrac{E_b}{E_0}\right)^{p_2 - p_1}\left(\dfrac{E}{E_0}\right)^{-p_2} & E > E_b, \end{cases} \quad (1)$$

2. Exponential cutoff power law:

$$N_0(E) = A_0 \left(\frac{E}{E_0}\right)^{-p_0} \exp\left[-\left(\frac{E}{E_c}\right)^{\beta}\right], \quad (2)$$

where $E_0 = 1$ TeV. β is fixed to 2, in which the electrons are accelerated up to 100 TeV and beyond and the maximum energy of electron resulted from the competition between the acceleration and energy loss rates
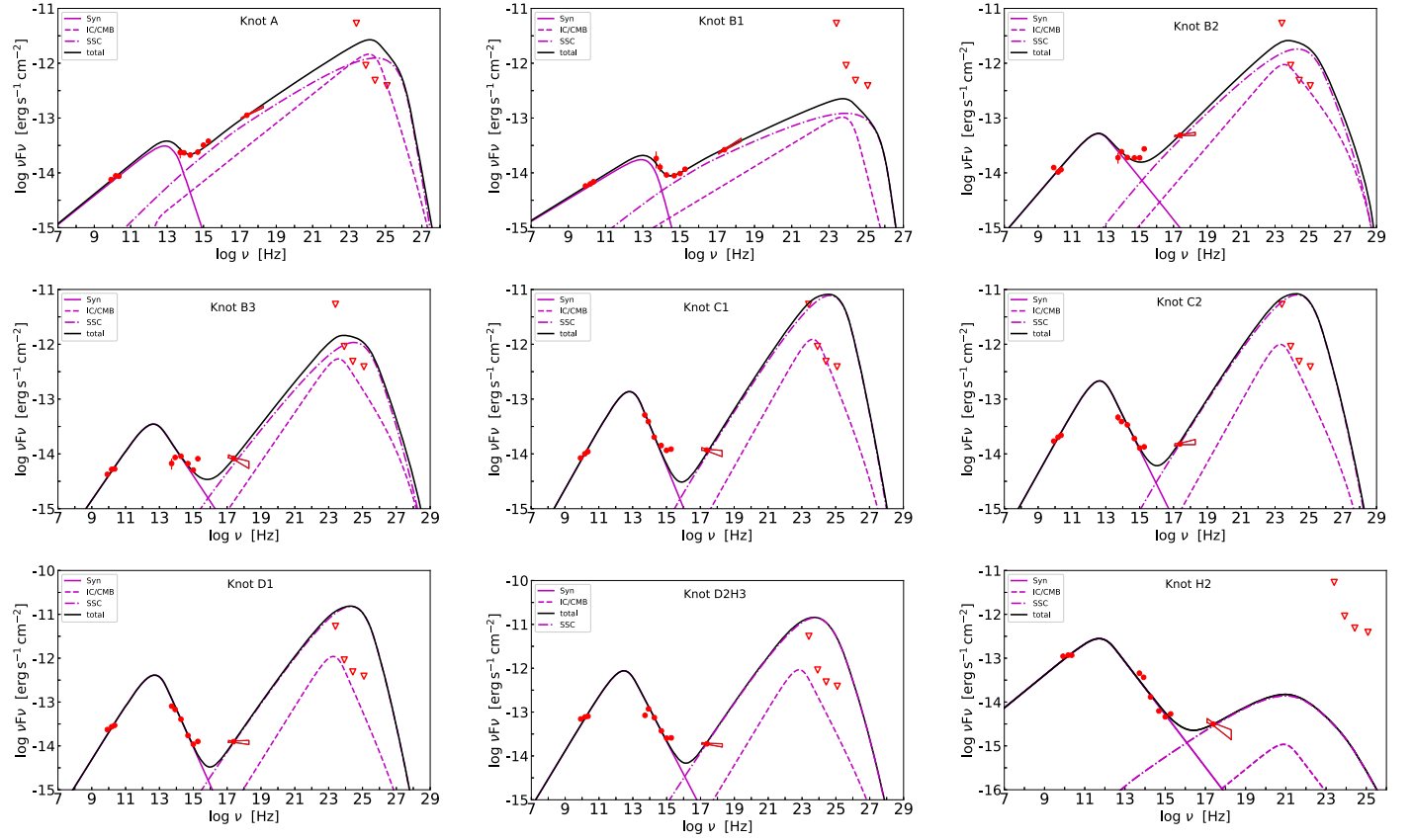
Figure 1. Observed broadband SEDs (circles, bowties, and triangles) of the jet knots together with the model fits (black solid lines) of a single-electron population (scenario I) for the $\delta = 1$ case. The purple solid, dashed–dotted, and dashed lines display the synchrotron radiation, SSC, and IC/CMB components, respectively. The upper-limit data (red opened triangles) observed by the Fermi/LAT are taken from Meyer et al. (2015).

(Zirakashvili & Aharonian 2007; Aharonian et al. 2017).

We consider three scenarios in our SED fits: a single-electron population, two-electron populations, and an electron population plus a proton population. The numerical package of Naima (Zabalza 2015), which includes a set of nonthermal radiation models and the spectral fitting procedure, is used in this paper. The best-fit and uncertainty of the model parameters are derived via the Markov Chain Monte Carlo (Foreman-Mackey et al. 2013) method.

2.1. Scenario I: A Single Electron Population

In this scenario, the synchrotron, SSC, and IC/CMB radiation of a single-electron population are used to reproduce the broadband SEDs of knots. The radiating electrons are assumed to have the number distribution seen in Equation (1). The minimum and maximum energies of electrons are taken as $E_{\rm e,min} = 1\,{\rm MeV}$, and $E_{\rm e,max} = 510\,{\rm TeV}$, which respectively correspond to $\gamma_{\rm e} \sim 2$ and $\gamma_{\rm e} \sim 10^9$, where $\gamma_{\rm e}$ is the Lorenz factor of electrons. If the knots do not have relativistic motions, i.e., $\delta = \Gamma = 1$, the IC component is dominated by the SSC process since the energy density of the synchrotron radiation photon field ($U_{\rm syn}$) is higher than $U'_{\rm CMB}$. A magnetic field strength (B) lower than the equipartition value ($B_{\rm eq}$) is also needed (e.g., Kataoka & Stawarz 2005; Harris & Krawczynski 2006; Zhang et al. 2010, 2018a), thus we do not take the equipartition condition into account in this scenario. The free parameters of the SED modeling are B, A_1, p_1, p_2, $E_{\rm b}$. The SED

fitting results are shown in Figure 1 and the derived parameters are listed in Table 1. In case these knots have relativistic motions toward us, i.e., $\delta > 1$, the IC/CMB process may dominate the high-energy emission of the SEDs. The equipartition condition is usually taken into account to constrain the model parameters, i.e., the energy density of relativistic electrons ($U_{\rm e}$) equal to the energy density of magnetic fields (U_B). Thus, the free parameters in the SED modeling are δ (or Γ), A_1, p_1, p_2, $E_{\rm b}$. The SED fitting results are displayed in Figure 2 and the derived parameters are listed in Table 1.

As illustrated in Figures 1 and 2, although the X-rays together with the UV emission of knot-A and knot-B1 can be explained with a single-electron population via the IC processes for $\delta = 1$ or $\delta > 1$, the SEDs of the other knots cannot be represented in this scenario.

2.2. Scenario II: Two-electron Populations

In this scenario, we add another electron population and try to explain the broadband SEDs with the synchrotron radiations of two-electron populations, i.e., an exponential cutoff power-law electron population (Equation (2)) plus a broken power-law electron population. The minimum and maximum energies of electrons in the two-electron populations are taken as $E_{\rm e,min} = 1\,{\rm MeV}$ and $E_{\rm e,max} = 510\,{\rm TeV}$. We assume that the two-electron populations are totally independent (see also Zargaryan et al. 2017; Sun et al. 2018) and riskily assume that the two radiation regions of an individual knot have the same size with $R_1 = R_2 = R$ to calculate the equipartition magnetic
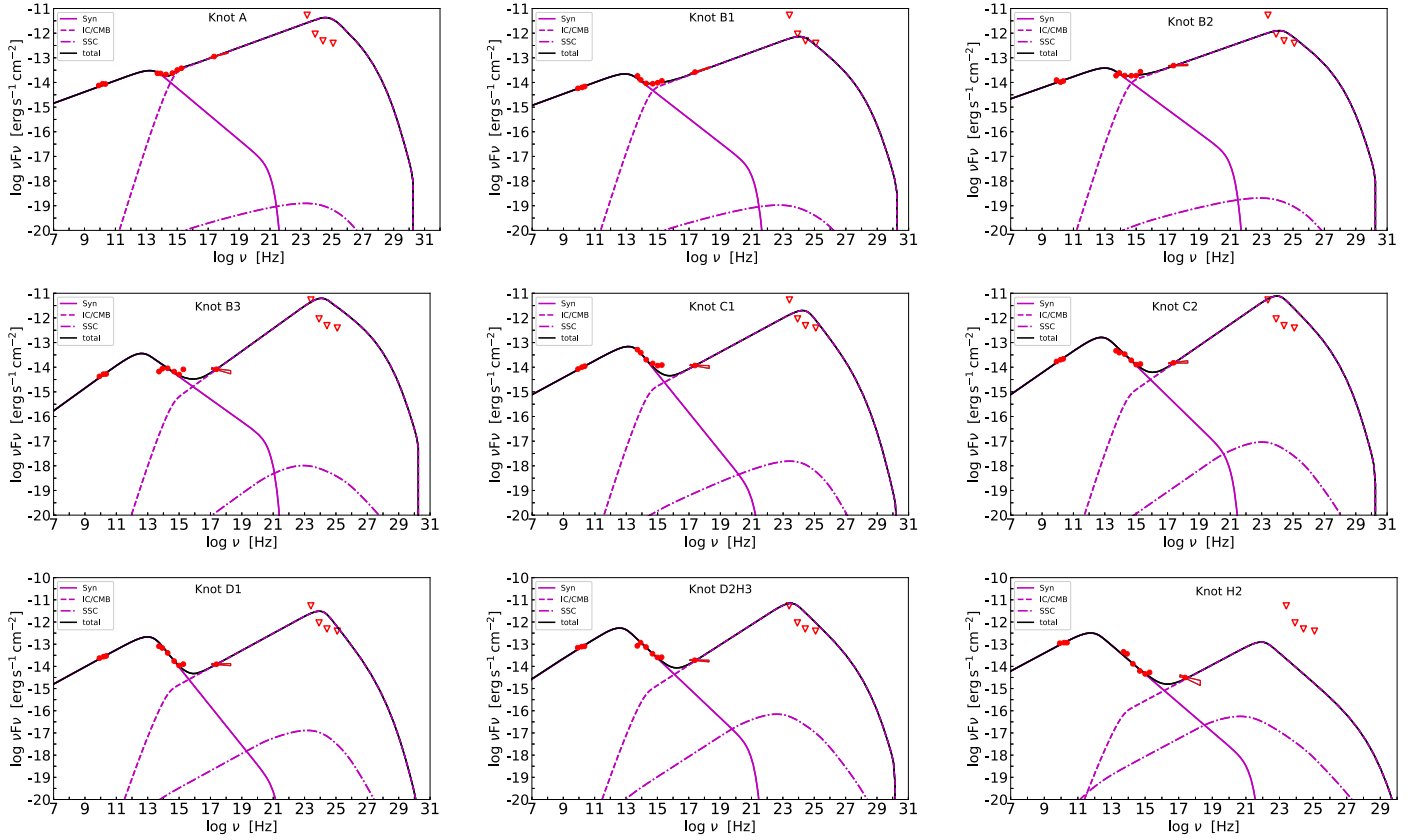
Figure 2. Same as Figure 1, but for the model fits of a single-electron population (scenario I) for the $\delta > 1$ case.

field strength, i.e., $U_B = U_e$. The two synchrotron components are calculated under the equipartition condition. For $\delta = 1$, the free parameters of the SED modeling are A_0, p_0, E_c, A_1, p_1, p_2, E_b. The SED fitting results are shown in Figure 3 and the corresponding SSC and IC/CMB contributions of two-electron populations are also presented in Figure 3. The fitting parameters are reported in Table 2.

In the $\delta > 1$ case, the model loses the constraint on the δ value since there is no observation of the IC component in these knots. We adopt $\delta = 3.7$ (the variability Doppler factor in Liodakis et al. 2017) and $\theta = 3°.3$ (Hovatta et al. 2009), and thus obtain $\Gamma = 2$, which is consistent with $\Gamma < 2.9$ by assuming that the large-scale jet knots are packets of moving plasma with an upper limit of $1c$ (Meyer et al. 2016). In this case, the free parameters of the SED modeling are A_0, p_0, E_c, A_1, p_1, p_2, E_b. The SED fitting results are shown in Figure 4 and the corresponding SSC and IC/CMB contributions of two-electron populations are also presented in Figure 4. The fitting parameters are listed in Table 2. The model can reproduce the broadband SEDs of knots in both the $\delta = 1$ and $\delta > 1$ cases.

2.3. Scenario III: An Electron Population Plus a Proton Population

It was suggested that the X-ray emission of large-scale jets in some AGNs may be from the synchrotron radiation of protons (e.g., Aharonian 2002; Kundu & Gupta 2014). We thus try to explain the X-ray emission with the synchrotron radiation of the accelerated protons in these knots, i.e., the synchrotron radiations of an exponential cutoff power-law electron population (Equation (2)) and a broken power-law proton population (Equation (1)) are considered in this scenario. The minimum

and maximum energies of electrons and protons are $E_{e,min} = 1\,MeV$, $E_{e,max} = 200\,TeV$, $E_{p,min} = 100\,TeV$, and $E_{p,max} = 5\,EeV$, respectively, where the minimum energy of protons roughly results in equal numbers of electrons and protons in the knots. The equipartition magnetic field strength is calculated with $U_B = U_e + U_p$, where U_p is the energy density of nonthermal protons. In the $\delta = 1$ case, the free parameters of the SED modeling are A_0, p_0, E_c, A_1, p_1, p_2, E_b. The SED fitting results are shown in Figure 5 and the corresponding SSC and IC/CMB contributions of the electron population are also presented in Figure 5. The fitting parameters are listed in Table 3.

The $\delta > 1$ case, following our approach for scenario II, we also adopt $\delta = 3.7$, $\theta = 3°.3$, and $\Gamma = 2$ in the SED modeling. Since the derived equipartition magnetic field strengths (as listed in Table 3) of knots are smaller than $1\,mG$, which conflicts with the condition that the energy loss of protons is dominated by the synchrotron cooling (see Section 3), we take $B = 5\,mG$ (see also Aharonian 2002) for all knots. In this case, the free parameters of the SED modeling are A_0, p_0, E_c, A_1, p_1, p_2, E_b. The SED fitting results are shown in Figure 6 and the corresponding SSC and IC/CMB contributions of the electron population are also presented in Figure 6. The fitting parameters are given in Table 3. The SEDs of knots can be represented by the model in either the $\delta = 1$ or $\delta > 1$ case.

3. Discussion

The above analysis shows that although the X-rays together with the UV emission of knot-A and knot-B1 can be explained with a single-electron population via the IC processes (Scenario I), in both the $\delta = 1$ and $\delta > 1$ cases, the broadband SEDs of
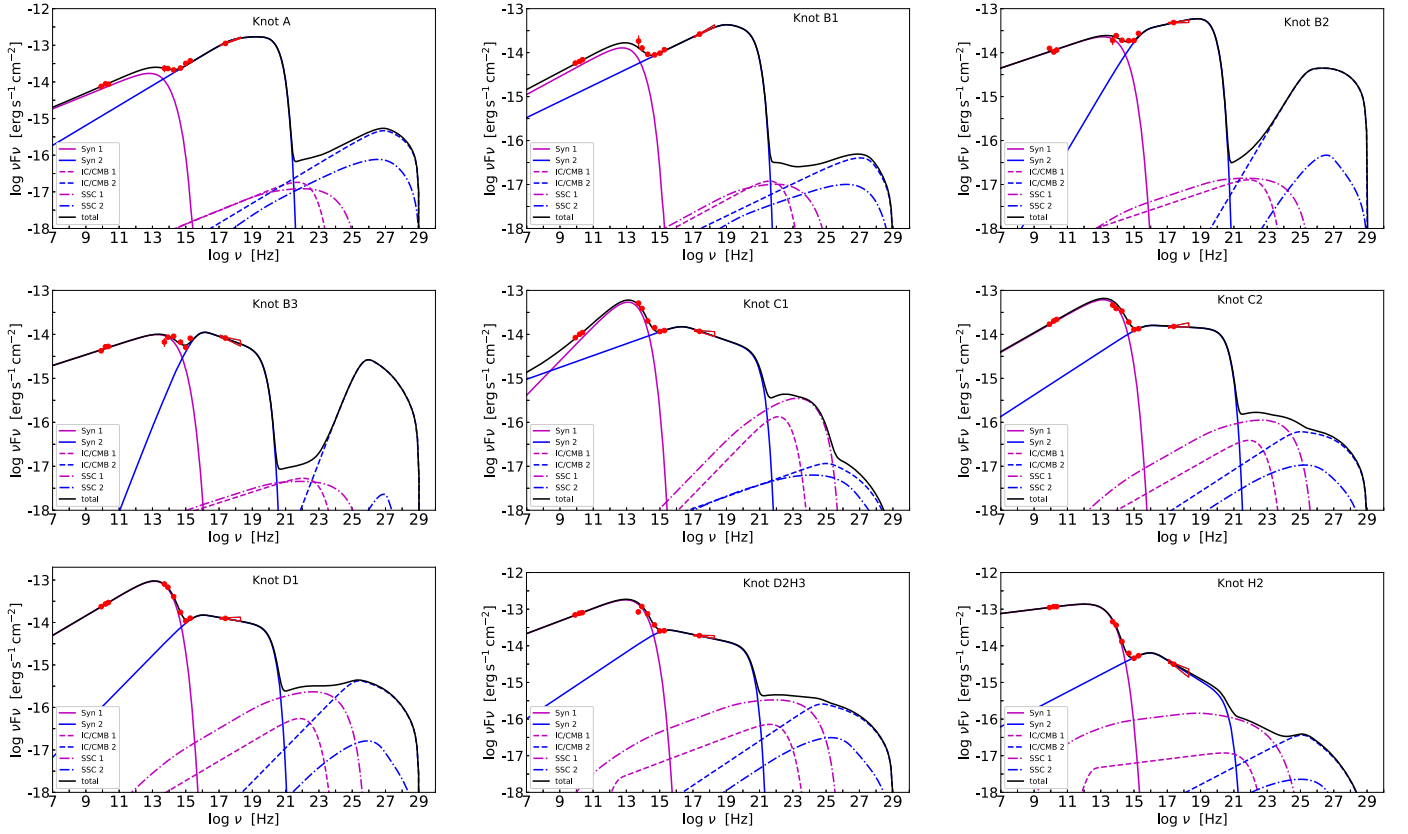
Figure 3. Same as Figure 1, but for the model fits of two-electron populations (scenario II) for the $\delta = 1$ case. The purple and blue lines display the radiation components from the two-electron populations.

Table 2
Parameters in the Scenario II: Two-electron Populations

Knot	A_0 (1/eV)	E_c (GeV)	p_0[a]	A_1 (1/eV)	E_b (TeV)	p_1	p_2[a]	E_{total} (erg)	$B_{eq,1}$ (μG)	$B_{eq,2}$ (μG)	$\log P_e$ (erg s^{-1})
$\delta = 1$											
A	$8.2^{+0.7}_{-1.2}$E40	164^{+5}_{-14}	2.63	$1.5^{+0.1}_{-0.3}$E41	25^{+3}_{-3}	$2.46^{+0.03}_{-0.02}$	$2.91^{+0.19}_{-0.15}$	$1.6^{+0.1}_{-0.1}$E57	157^{+4}_{-4}	75^{+8}_{-4}	45.71
B1	$6.5^{+0.4}_{-0.4}$E40	137^{+5}_{-3}	2.59	$2.2^{+0.2}_{-0.2}$E40	62^{+3}_{-5}	$2.63^{+0.02}_{-0.01}$	3.15	$9.6^{+0.4}_{-0.2}$E56	168^{+2}_{-2}	126^{+8}_{-6}	45.63
B2	$3.7^{+0.2}_{-0.2}$E40	252^{+9}_{-9}	2.75	$8.5^{+0.3}_{-0.3}$E41	$4.4^{+0.1}_{-0.1}$	$1.72^{+0.06}_{-0.1}$	$2.83^{+0.04}_{-0.03}$	$2.4^{+0.1}_{-2}$E57	216^{+2}_{-2}	14^{+1}_{-6}	45.90
B3	$1.4^{+0.3}_{-0.2}$E40	308^{+19}_{-19}	2.76	$1.3^{+0.1}_{-0.1}$E41	$6.2^{+0.7}_{-0.7}$	$1.03^{+0.06}_{-0.06}$	$3.26^{+0.11}_{-0.08}$	$1.1^{+0.1}_{-0.1}$E57	220^{+4}_{-4}	$9.9^{+0.1}_{-0.1}$	45.67
C1	$1.7^{+0.1}_{-0.1}$E42	176^{+8}_{-4}	2.22	$1.3^{+0.1}_{-0.1}$E40	$2.8^{+0.2}_{-0.1}$	$2.73^{+0.02}_{-0.02}$	$3.26^{+0.10}_{-0.10}$	$9.2^{+1.5}_{-1.1}$E56	104^{+4}_{-10}	179^{+20}_{-16}	45.62
C2	$1.9^{+0.1}_{-0.1}$E41	193^{+8}_{-3}	2.57	$6.2^{+0.1}_{-0.1}$E40	$1.9^{+0.1}_{-0.1}$	$2.51^{+0.02}_{-0.02}$	$3.04^{+0.04}_{-0.08}$	$1.6^{+0.1}_{-0.1}$E57	204^{+1}_{-5}	80^{+6}_{-10}	45.80
D1	$3.1^{+0.1}_{-0.3}$E41	174^{+1}_{-2}	2.54	$2.4^{+0.1}_{-0.1}$E41	$3.4^{+0.1}_{-0.1}$	$2.20^{+0.02}_{-0.01}$	$3.14^{+0.08}_{-0.03}$	$1.6^{+0.1}_{-0.1}$E57	212^{+1}_{-4}	29^{+2}_{-2}	45.78
D2H3	$3.0^{+0.2}_{-0.2}$E41	157^{+3}_{-2}	2.66	$2.8^{+0.1}_{-0.1}$E41	$1.6^{+0.1}_{-0.1}$	$2.39^{+0.01}_{-0.01}$	$3.19^{+0.08}_{-0.06}$	$6.8^{+0.2}_{-0.4}$E57	256^{+3}_{-7}	51^{+2}_{-5}	46.26
H2	$2.7^{+0.1}_{-0.1}$E40	$70.2^{+0.3}_{-0.2}$	2.89	$3.4^{+0.1}_{-0.4}$E40	$3.2^{+0.1}_{-0.2}$	$2.53^{+0.02}_{-0.01}$	$3.56^{+0.05}_{-0.05}$	$1.0^{+0.1}_{-0.1}$E58	544^{+2}_{-2}	66^{+5}_{-3}	46.59
$\delta = 3.7$											
A	$6.1^{+0.1}_{-0.1}$E39	170^{+1}_{-1}	2.63	$1.2^{+0.1}_{-0.1}$E40	$30^{+2}_{-3.0}$	$2.44^{+0.02}_{-0.02}$	$3.18^{+0.2}_{-0.14}$	$1.1^{+0.1}_{-0.1}$E56	$42.6^{+0.2}_{-0.2}$	$19.2^{+1.0}_{-1.0}$	45.17
B1	$4.7^{+0.2}_{-0.1}$E39	136^{+1}_{-1}	2.59	$1.6^{+0.1}_{-0.1}$E39	106^{+7}_{-7}	$2.63^{+0.01}_{-0.01}$	3.15	$6.8^{+0.3}_{-0.3}$E55	$45.2^{+0.9}_{-0.6}$	$33.4^{+0.8}_{-1.2}$	45.08
B2	$2.5^{+0.1}_{-0.1}$E39	259^{+7}_{-11}	2.76	$6.4^{+0.2}_{-0.2}$E40	$4.9^{+0.2}_{-0.2}$	$1.78^{+0.05}_{-0.05}$	$2.88^{+0.04}_{-0.04}$	$1.9^{+0.1}_{-0.1}$E56	$60.7^{+1.5}_{-1.5}$	$4.0^{+0.2}_{-0.2}$	45.40
B3	$4.3^{+0.1}_{-0.1}$E39	232^{+1}_{-1}	2.6	$2.0^{+0.1}_{-0.1}$E40	$5.8^{+0.3}_{-0.2}$	$1.70^{+0.04}_{-0.06}$	$3.18^{+0.02}_{-0.02}$	$4.6^{+0.1}_{-0.1}$E55	$46.2^{+0.5}_{-0.5}$	$3.2^{+0.1}_{-0.1}$	44.92
C1	$7.3^{+0.1}_{-0.1}$E40	171^{+3}_{-1}	2.3	$2.1^{+0.4}_{-0.3}$E39	$1.9^{+0.1}_{-0.1}$	$2.59^{+0.03}_{-0.03}$	$3.14^{+0.02}_{-0.02}$	$4.4^{+0.3}_{-0.3}$E55	$33.2^{+0.2}_{-0.3}$	31^{+2}_{-2}	44.89
C2	$1.7^{+0.1}_{-0.1}$E40	184^{+1}_{-1}	2.55	$4.7^{+0.1}_{-0.1}$E39	$1.2^{+0.1}_{-0.1}$	$2.51^{+0.01}_{-0.01}$	$3.00^{+0.01}_{-0.02}$	$1.2^{+0.1}_{-0.1}$E56	$53.5^{+0.7}_{-0.7}$	$22.5^{+1.0}_{-1.3}$	45.25
D1	$2.3^{+0.1}_{-0.1}$E40	175^{+1}_{-1}	2.54	$3.6^{+0.1}_{-0.1}$E40	$3.6^{+0.1}_{-0.1}$	$1.96^{+0.02}_{-0.03}$	$3.11^{+0.01}_{-0.01}$	$1.2^{+0.1}_{-0.1}$E56	$58.1^{+0.7}_{-1.0}$	$4.6^{+0.2}_{-0.2}$	45.25
D2H3	$1.4^{+0.1}_{-0.1}$E40	169^{+1}_{-1}	2.71	$2.1^{+0.1}_{-0.1}$E40	$1.7^{+0.1}_{-0.1}$	$2.37^{+0.01}_{-0.02}$	$3.17^{+0.06}_{-0.02}$	$5.8^{+0.1}_{-0.1}$E56	$75.4^{+0.1}_{-0.1}$	$12.5^{+0.3}_{-1.0}$	45.79
H2	$1.9^{+0.1}_{-0.1}$E39	$70^{+0.1}_{-0.2}$	2.89	$2.4^{+0.1}_{-0.2}$E39	$3.0^{+0.1}_{-0.7}$	$2.53^{+0.02}_{-0.01}$	$3.55^{+0.08}_{-0.08}$	$7.6^{+0.2}_{-0.2}$E56	148^{+2}_{-2}	$17.7^{+0.9}_{-0.7}$	46.07

Note.

[a] p_0 is not fixed during SED fits, but the derived errors are ~0.01 and thus are not shown in the table. p_2 of knot-B1 is fixed as the average value of other knots.
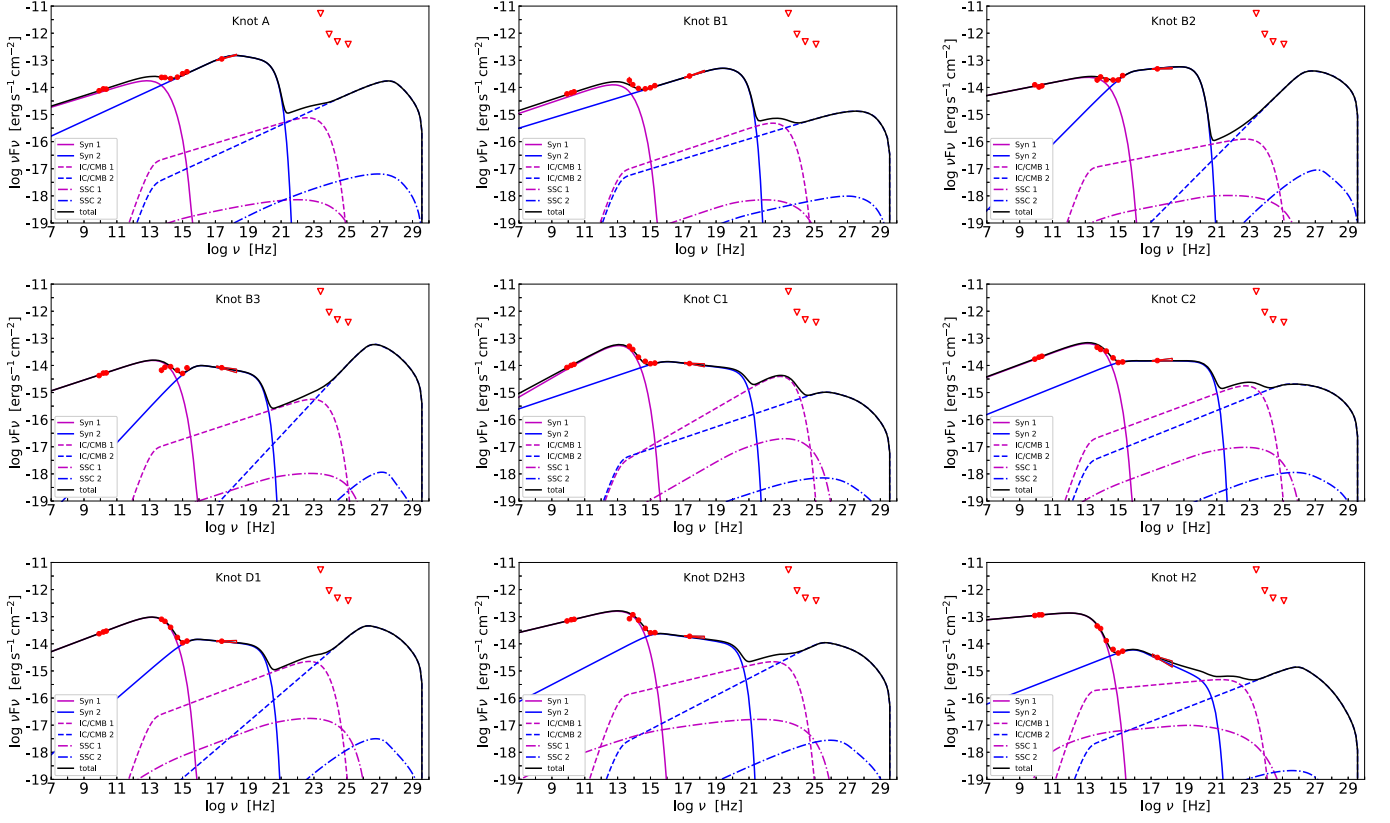
Figure 4. Same as Figure 1, but for the model fits of two-electron populations (scenario II) in the $\delta > 1$ case. The purple and blue lines display the radiation components from the two-electron populations.
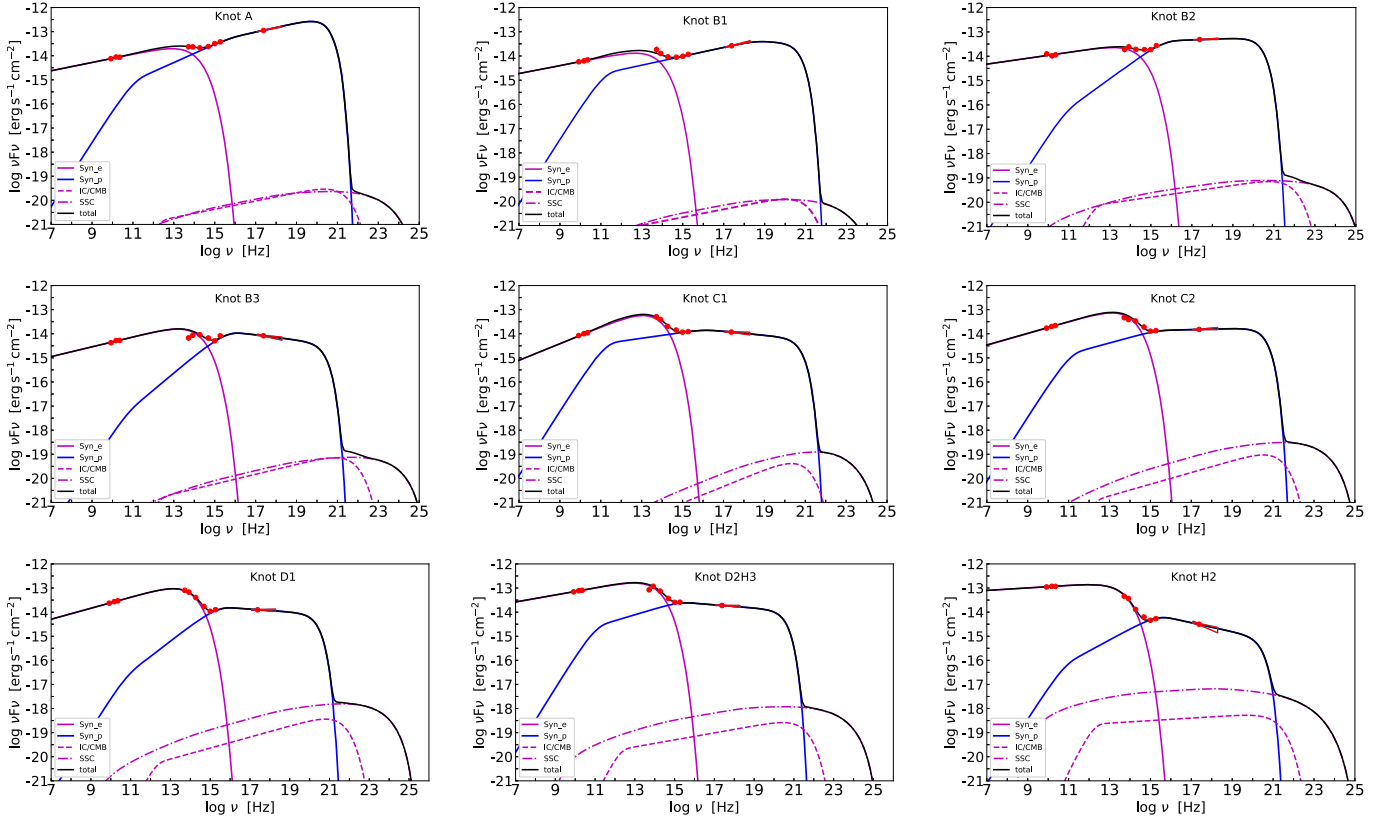

Figure 5. Same as Figure 1, but for the model fits of an electron population plus a proton population (scenario III) in the $\delta = 1$ case. The purple and blue lines display the radiation components from the electron population and the proton population, respectively.

Table 3
Parameters in the Scenario III: An Electron Population Plus a Proton Population

Knot	A_0 (1/eV)	E_c (GeV)	p_0[a]	A_1 (1/eV)	E_b (PeV)	p_1	p_2[a]	$E_{e,total}$ (erg)	$E_{p,total}$ (erg)	B[b] (μG)	B_{eq} (μG)	$\log P_e$ (erg s^{-1})	$\log P_p$ (erg s^{-1})
$\delta = 1$													
A	$2.0^{+0.1}_{-0.1}$E38	$36.6^{+0.5}_{-0.7}$	2.66	$4.9^{+0.1}_{-0.2}$E47	$28.4^{+1.5}_{-0.7}$	$2.24^{+0.01}_{-0.01}$	$2.62^{+0.03}_{-0.02}$	$9.5^{+0.1}_{-0.1}$E53	$9.1^{+0.1}_{-0.1}$E59	4204^{+10}_{-15}	4204^{+10}_{-15}	42.50	48.48
B1	$9.1^{+0.7}_{-0.5}$E37	$25.5^{+0.4}_{-0.4}$	2.67	$4.4^{+0.2}_{-0.2}$E48	540^{+20}_{-20}	$2.63^{+0.01}_{-0.01}$	3.07	$4.8^{+0.1}_{-0.1}$E53	$6.0^{+0.1}_{-0.1}$E59	5280^{+30}_{-30}	5280^{+30}_{-30}	42.33	48.43
B2	$2.7^{+0.1}_{-0.1}$E38	72^{+3}_{-5}	2.76	$5.7^{+0.2}_{-0.3}$E45	$30.7^{+0.6}_{-0.4}$	$1.77^{+0.01}_{-0.01}$	$2.93^{+0.03}_{-0.02}$	$1.9^{+0.1}_{-0.1}$E51	$4.3^{+0.1}_{-0.1}$E59	2880^{+30}_{-20}	2880^{+30}_{-20}	39.80	48.15
B3	$5.4^{+0.2}_{-0.2}$E38	$61.2^{+0.8}_{-0.8}$	2.59	$3.1^{+0.1}_{-0.1}$E44	$31.3^{+1.0}_{-2.0}$	$1.57^{+0.01}_{-0.01}$	$3.21^{+0.04}_{-0.05}$	$7.2^{+0.1}_{-0.1}$E50	$1.2^{+0.1}_{-0.1}$E59	2388^{+8}_{-11}	2388^{+8}_{-11}	39.50	47.74
C1	$1.6^{+0.1}_{-0.1}$E39	$23.9^{+0.2}_{-0.2}$	2.31	$1.3^{+0.1}_{-0.1}$E49	$29.7^{+0.9}_{-0.4}$	$2.76^{+0.01}_{-0.01}$	$3.16^{+0.01}_{-0.01}$	$2.7^{+0.1}_{-0.1}$E53	$8.0^{+0.1}_{-0.1}$E59	6086^{+16}_{-30}	6086^{+16}_{-30}	42.08	48.55
C2	$1.2^{+0.1}_{-0.1}$E39	$36.5^{+0.7}_{-0.4}$	2.51	$2.9^{+0.1}_{-0.1}$E48	$14.9^{+0.3}_{-0.3}$	$2.54^{+0.01}_{-0.01}$	$2.96^{+0.01}_{-0.02}$	$1.4^{+0.1}_{-0.1}$E54	$7.1^{+0.1}_{-0.1}$E59	4541^{+15}_{-15}	4541^{+15}_{-15}	42.72	48.43
D1	$3.5^{+0.1}_{-0.1}$E39	$51.1^{+0.3}_{-0.3}$	2.54	$2.4^{+0.1}_{-0.1}$E45	$23.2^{+0.3}_{-0.3}$	$1.72^{+0.01}_{-0.01}$	$3.12^{+0.01}_{-0.01}$	$2.9^{+0.1}_{-0.1}$E51	$2.3^{+0.1}_{-0.1}$E59	2601^{+16}_{-6}	2601^{+16}_{-6}	40.05	47.95
D2H3	$1.4^{+0.1}_{-0.1}$E39	$43.8^{+0.5}_{-0.7}$	2.7	$5.5^{+0.1}_{-0.1}$E48	$14.4^{+0.2}_{-0.2}$	$2.51^{+0.01}_{-0.01}$	$3.13^{+0.02}_{-0.02}$	$1.1^{+0.1}_{-0.1}$E55	$1.6^{+0.1}_{-0.1}$E60	4000^{+30}_{-20}	4000^{+30}_{-20}	43.46	48.63
H2	$1.2^{+0.1}_{-0.1}$E39	$33.0^{+0.4}_{-0.2}$	2.9	$4.2^{+0.1}_{-0.1}$E46	$20.9^{+0.9}_{-1.9}$	$2.08^{+0.01}_{-0.01}$	$3.37^{+0.04}_{-0.04}$	$6.5^{+0.2}_{-0.1}$E55	$2.3^{+0.1}_{-0.1}$E59	2587^{+16}_{-40}	2587^{+16}_{-40}	44.40	47.94
$\delta = 3.7$													
A	$1.2^{+0.1}_{-0.1}$E36	$16.2^{+0.1}_{-0.1}$	2.63	$4.5^{+0.2}_{-0.3}$E45	$20.6^{+1.2}_{-1.2}$	$2.28^{+0.01}_{-0.01}$	$2.68^{+0.01}_{-0.01}$	$1.9^{+0.1}_{-0.1}$E52	$6.2^{+0.1}_{-0.1}$E57	5000	348^{+2}_{-3}	41.40	46.92
B1	$1.3^{+0.1}_{-0.1}$E36	$12.4^{+0.2}_{-0.1}$	2.59	$3.2^{+0.2}_{-0.1}$E46	400^{+50}_{-50}	$2.63^{+0.01}_{-0.01}$	3.07	$1.2^{+0.1}_{-0.1}$E52	$4.5^{+0.1}_{-0.1}$E57	5000	456^{+4}_{-4}	41.33	46.90
B2	$5.8^{+0.1}_{-0.1}$E35	$28.7^{+1.1}_{-0.4}$	2.76	$8.8^{+0.6}_{-0.4}$E43	$15.8^{+0.8}_{-0.8}$	$1.89^{+0.01}_{-0.01}$	$2.99^{+0.02}_{-0.02}$	$2.4^{+0.1}_{-0.1}$E49	$2.0^{+0.1}_{-0.1}$E57	5000	195^{+3}_{-5}	38.51	46.42
B3	$9.3^{+0.1}_{-0.1}$E35	$22.5^{+0.2}_{-0.2}$	2.6	$4.6^{+0.1}_{-0.4}$E41	10^{+3}_{-2}	$1.43^{+0.01}_{-0.02}$	$3.19^{+0.12}_{-0.12}$	$5.4^{+0.1}_{-0.1}$E48	$3.7^{+0.1}_{-0.1}$E56	5000	130^{+1}_{-1}	37.98	45.81
C1	$2.1^{+0.1}_{-0.1}$E37	$13.3^{+0.1}_{-0.1}$	2.3	$1.1^{+0.1}_{-0.1}$E47	$15.7^{+0.4}_{-0.4}$	$2.75^{+0.01}_{-0.01}$	$3.15^{+0.01}_{-0.01}$	$6.6^{+0.1}_{-0.1}$E51	$7.2^{+0.2}_{-0.2}$E57	5000	579^{+5}_{-9}	41.07	47.11
C2	$5.6^{+0.1}_{-0.1}$E36	$19.0^{+0.2}_{-0.2}$	2.55	$1.6^{+0.1}_{-0.1}$E46	$7.1^{+0.3}_{-0.3}$	$2.53^{+0.01}_{-0.01}$	$2.95^{+0.01}_{-0.01}$	$3.2^{+0.1}_{-0.1}$E52	$4.1^{+0.1}_{-0.1}$E57	5000	347^{+3}_{-3}	41.69	46.80
D1	$8.2^{+0.1}_{-0.1}$E36	$19.0^{+0.1}_{-0.1}$	2.54	$2.3^{+0.2}_{-0.2}$E43	$8.5^{+0.3}_{-0.3}$	$1.79^{+0.01}_{-0.01}$	$3.10^{+0.01}_{-0.01}$	$2.3^{+0.1}_{-0.1}$E49	$9.1^{+0.1}_{-0.1}$E56	5000	163^{+1}_{-1}	38.54	46.14
D2H3	$5.8^{+0.1}_{-0.1}$E36	$20.6^{+0.1}_{-0.1}$	2.71	$1.1^{+0.1}_{-0.1}$E46	$7.2^{+0.3}_{-0.3}$	$2.40^{+0.01}_{-0.01}$	$3.16^{+0.04}_{-0.03}$	$2.4^{+0.1}_{-0.1}$E53	$6.0^{+0.1}_{-0.1}$E57	5000	245^{+2}_{-2}	42.41	46.80
H2	$2.0^{+0.1}_{-0.1}$E36	$12.2^{+0.1}_{-0.1}$	2.89	$1.7^{+0.2}_{-0.2}$E44	$5.4^{+1.7}_{-1.1}$	$2.07^{+0.01}_{-0.01}$	$3.28^{+0.05}_{-0.05}$	$8.0^{+0.1}_{-0.1}$E53	$7.8^{+0.7}_{-0.7}$E56	5000	151^{+7}_{-7}	43.08	46.07

Notes.

[a] p_0 is not fixed during SED fits, but the derived errors are ~0.01 and thus are not shown in the table. p_2 of knot-B1 is fixed as the average value of other knots.

[b] $B = B_{eq}$ in the $\delta = 1$ case, but $B = 5$ mG the $\delta > 1$ case; for more details see the text.
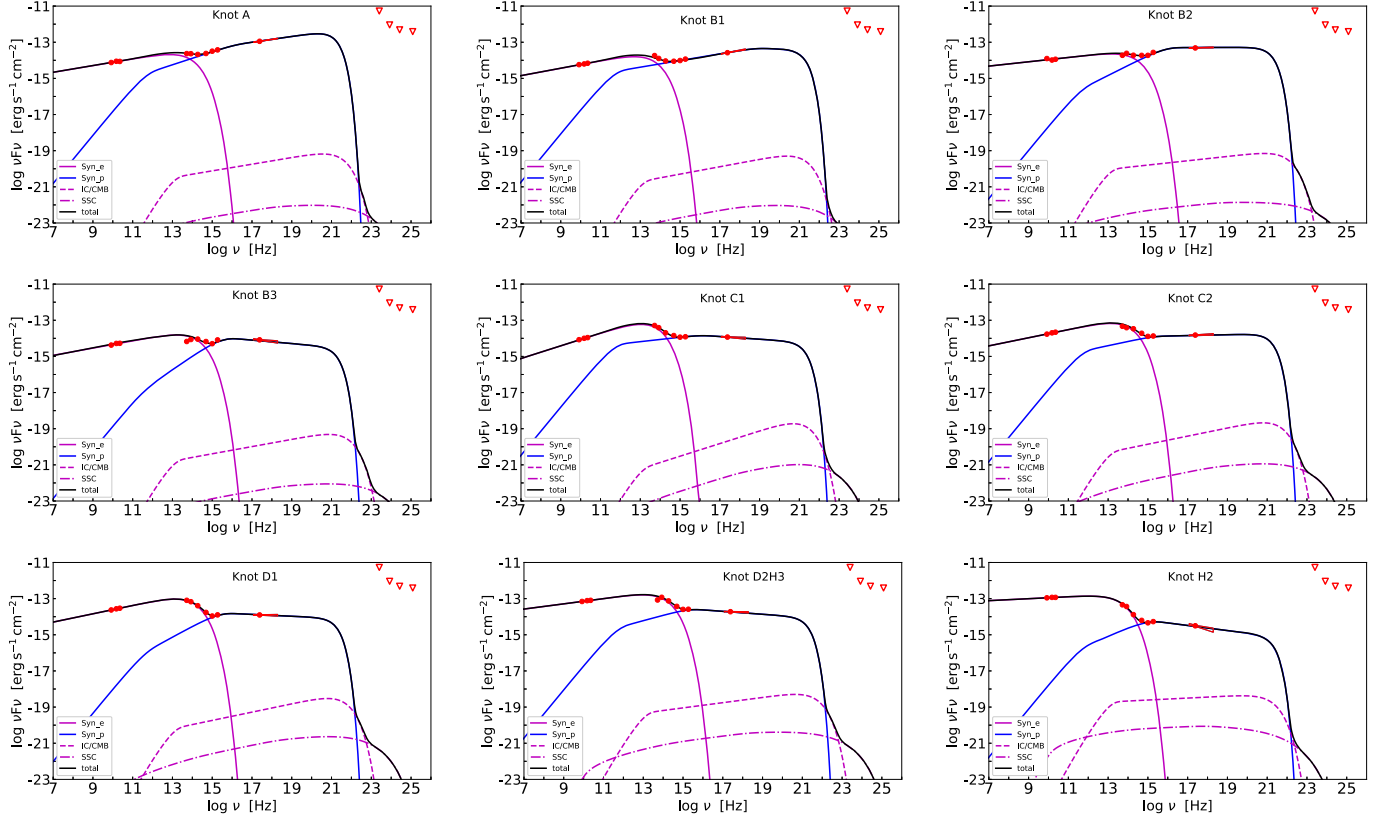
Figure 6. Same as Figure 1, but for the model fits of an electron population plus a proton population (scenario III) for the $\delta > 1$ case. The purple and blue lines display the radiation components from the electron population and the proton population, respectively.

the other knots cannot be represented in this scenario. In this scenario, the predicted γ-ray flux is normally much higher than the upper limits set by Fermi/LAT observations, such as that seen in knot-A. This is also a reason to rule out the IC/CMB model for the large-scale jet of 3C 273 (Meyer et al. 2015). The SED of knot-B1 apparently can be represented in this scenario, but the derived B value is 1.83 μG in the $\delta = 1$ case, which is much lower than the derived equipartition magnetic field strength of $B_{eq} = 10.5$ mG. Zhang et al. (2018a) suggested that using the SSC process to explain the X-ray emission of large-scale jet substructures would result in an extremely high jet power. We estimate the powers of the nonthermal electrons using $P_e = \pi R^2 \Gamma^2 c U_e$ (see also Zargaryan et al. 2017 for the large-scale jet knots), and find that P_e ranges from 3.0×10^{46} to 2.3×10^{49} erg s^{-1} in the $\delta = 1$ case for the knots (as shown in Table 1). The black hole mass of 3C 273 is $10^{9.693} M_\odot$ (Gu et al. 2001) and the corresponding Eddington luminosity is 6.2×10^{47} erg s^{-1}. P_e is $\sim 10^{49}$ erg s^{-1} for knot-B1, which is far beyond the Eddington luminosity of the source. In the $\delta > 1$ case, a large δ value ($\delta = 16.6$) is required to model the SED of knot-B1. This value is comparable with the derived variability Doppler factor of $\delta = 17$ for a parsec-scale jet in Hovatta et al. (2009), but is much larger than that reported by Liodakis et al. (2017, $\delta = 3.7$), and even larger than the core-jet value of $\delta = 7.4 \pm 0.9$ derived by SED fitting (Zhang et al. 2014, 2015). Therefore, Scenario I could not provide a reasonable explanation for the SEDs of knots.

The scenario of two-electron populations (Scenario II) can represent the SEDs in either the $\delta = 1$ or $\delta > 1$ case. Figure 7 illustrates the distributions of the derived parameters along the jet. We do not find any evolution feature for the parameters.

The medians of E_c and E_b are ~ 170 GeV and 4 TeV, respectively, indicating that the electrons are effectively accelerated. Note that the synchrotron cooling time of electrons is $t_{cool} = \frac{6\pi m_e^2 c^4}{\sigma_T c E_e B^2}$, and the electron travel distance can be estimated from $ct_{cool} \sim 3850 E_{e,TeV}^{-1} B_{\mu G}^{-2}$ kpc, where the electron energy ($E_{e,TeV}$) is in units of TeV and magnetic field strength ($B_{\mu G}$) is in units of μG. The high-energy electrons cannot travel more than 1 kpc before exhausting their energies owing to synchrotron cooling, and thus the electrons should be accelerated in situ. Except for knot-B2 and knot-B3, p_0 and p_1 of other knots are roughly consistent with the particle acceleration and cooling in shocks, hence the acceleration mechanisms of the two-electron populations may be the same. One can find that $B_{eq,1}$ of knot-H2 is higher than other knots. The substructure H2 in fact is historically labeled a hotspot and has a higher flux ratio of radio to X-ray than other knots. As reported by Zhang et al. (2010, 2018a), the observed luminosity ratio of radio to X-ray can help distinguish between hotspots and knots. In this scenario, P_e is from 4.2×10^{45} to 3.9×10^{46} erg s^{-1} in the $\delta = 1$ case and from 7.8×10^{44} to 1.2×10^{46} erg s^{-1} in the of $\delta > 1$ case among the knots. Although it has been suggested that the X-ray emission could be from the synchrotron radiation of an additional shock-accelerated electron population (Hardcastle 2006; Jester et al. 2006; Uchiyama et al. 2006; Zargaryan et al. 2017), it is not known what physical process could produce the second electron population in a single radiation region. Although there is some observational evidence of the complex morphologies of the knots in 3C 273 (e.g., Jester et al. 2005), no compact subcomponent, similar to in the hotspot of Pictor A
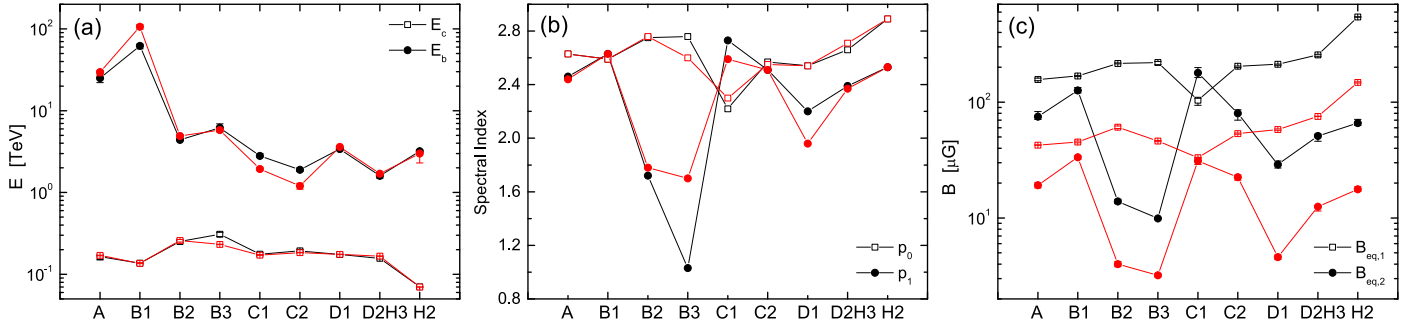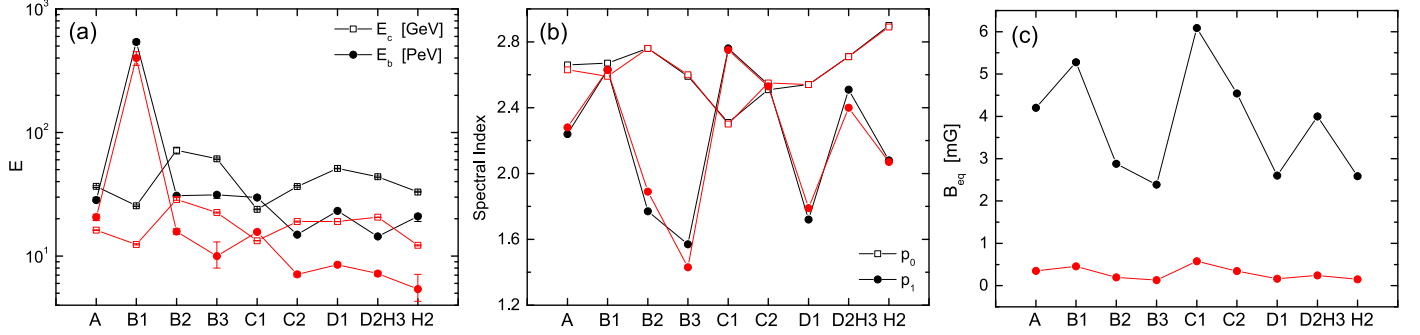
Figure 7. Parameter distributions along the jet derived by the model fits of two-electron populations (scenario II) in the $\delta = 1$ (black symbols) and $\delta > 1$ (red symbols) cases, including the cutoff energy (E_c) of the exponential cutoff power-law electron spectrum and the break energy (E_b) of the broken power-law electron spectrum, the spectral indices (p_0 and p_1) of the two-electron population distributions, and the equipartition magnetic field strengths ($B_{eq,1}$ and $B_{eq,2}$) of the two zones for each knot.

Figure 8. Parameter distributions along the jet derived by the model fits of an electron population plus a proton population (scenario III) in the $\delta = 1$ (black symbols) and $\delta > 1$ (red symbols) cases, including the cutoff energy (E_c) of the exponential cutoff power-law electron spectrum and the break energy (E_b) of the broken power-law proton spectrum, the spectral indices of electron population (p_0) and proton population (p_1), and the equipartition magnetic field strengths (B_{eq}) for each knot.

(Tingay et al. 2008; Zhang et al. 2009), is observationally resolved in the knots to support two radiation regions. Due to severe synchrotron cooling, the high-energy electrons that contribute the X-ray emission could not propagate far from their birth/acceleration places. Consequently, the X-ray morphologies of these knots should be like point-sources, unless there are multiple compact regions inside the knots to accelerate electrons, as expected by the multi-zone leptonic model.

The scenario of an electron population plus a proton population (Scenario III) also reproduces the SEDs of knots well. In the $\delta = 1$ case, E_c of the electron spectra narrowly clusters at 24–72 GeV while E_b of the proton spectra is in the range of 14–32 PeV, except for knot-B1 with $E_b \sim 540$ PeV, i.e., $\gamma_p \sim 10^7$, where γ_p is the Lorentz factors of protons. The X-ray spectrum of knot-B1 perfectly agrees with the extrapolation of its optical–UV spectrum, as displayed in Figure 5, thus a large peak energy is presented in the broadband SED and results in a large E_b. In the $\delta > 1$ case, the derived equipartition magnetic fields of knots are smaller than 1 mG (as listed in Table 3) and $B = 5$ mG is taken in our SED fitting. Hence, the knots would deviate from the equipartition condition if the X-ray emission is dominated by the synchrotron radiation of protons. We also illustrate the distributions of the derived parameters along the jet in Figure 8 and do not find any evolution feature for the parameters. In this scenario, the powers of radiation particles are dominated by the powers of nonthermal protons (P_p), which is estimated using $P_p = \pi R^2 \Gamma^2 c U_p$. P_p ranges from 5.5×10^{47} to 4.3×10^{48} erg s^{-1} in the $\delta = 1$ case and ranges from 6.5×10^{45} to 1.3×10^{47} erg s^{-1} in the $\delta > 1$ case. It seems likely that the

jet powers derived on large scales using the hadronic model parameters are super-Eddington in the $\delta = 1$ case. However, one can see that the total energies of radiation particles for these knots are significantly reduced in the presence of a relativistic bulk flow (see also Aharonian 2002).

For Scenario III, a maximum proton energy of 5 EeV is required to explain the X-ray emission of the knots. Rachen & Biermann (1993) reported that protons can even be accelerated by the mildly relativistic jet terminal shocks up to 100 EeV in hotspots with a magnetic field of ~ 0.5 mG and size of ~ 1 kpc. The observations with the very long baseline interferometry technique have demonstrated that the blazar jets are accelerated to relativistic velocities (e.g., Lister et al. 2009, 2019), thus they could produce strong shocks in the ambient medium. These shocks have been confirmed to propagate to kiloparsec scales in powerful (Nulsen et al. 2005; Simionescu et al. 2009; Gitti et al. 2010; Croston et al. 2011) and even less powerful jets (Kraft et al. 2007; Perucho et al. 2014, and references therein). Protons can also be accelerated to extremely high energies at the jet shear boundary layer (Ostrowski 1998). Hence, the protons in large-scale jet knots can be accelerated up to several EeV.

Note that ultra-high-energy cosmic rays (UHECRs) above 1 EeV have a predominant extragalactic origin component (e.g., Pierre Auger Collaboration et al. 2013; Aab et al. 2018), in which the energy range of 10^{18}–$10^{18.5}$ eV is dominated by protons (Abbasi et al. 2017; Schröder et al. 2019), and AGNs, especially blazars, may have UHECR origins. The escape time and the synchrotron cooling time of the high-energy protons

(Aharonian 2002), respectively, are

$$t_{esc} \simeq 4.2 \times 10^5 \eta^{-1} B_{mG} R_{kpc}^2 E_{19}^{-1} \text{ yr}, \quad (3)$$

$$t_{syn} \simeq 1.4 \times 10^7 B_{mG}^{-2} E_{19}^{-1} \text{ yr}, \quad (4)$$

where $\eta = 1$ is the gyrofactor in the Bohm limit, B_{mG} is the magnetic field strength in units of mG, R_{kpc} is the size of knots in units of kpc, and E_{19} is the proton energy in units of 10^{19} eV. If the protons are cooled down by the synchrotron radiation before escape, then $B_{mG}^3 R_{kpc}^2 \eta^{-1} \geqslant 34$. Taking a knot size of ~ 1 kpc in the Bohm regime $\eta = 1$ requires $B > 3$ mG. As listed in Table 3, the derived equipartition magnetic field strengths cluster at 2.4–6.1 mG in the $\delta = 1$ case, and the knots are larger than 1 kpc, so the high-energy protons that contribute to the X-ray emission would be cooled down by the synchrotron radiation before escape. However, the derived equipartition magnetic field strengths of knots would be smaller than 1 mG in *the* $\delta > 1$ case, hence the knots would deviate from the equipartition condition if the X-ray emission were dominated by the synchrotron radiation of protons. Note that the cooling times of the pp and pγ interactions are much longer than the escape time and the proton synchrotron cooling time, and the plasma density in knots should be at least 0.1–1 cm^{-3} for the effective pp interaction (Aharonian 2002), hence the synchrotron radiation of secondary electrons is not considered in this paper.

The X-ray emission of knot-A was previously explained with proton synchrotron radiations (Aharonian 2002; Kundu & Gupta 2014). Aharonian (2002) assumed the continuous injection of relativistic protons with a constant rate during the jet age (3×10^7 yr; see also Kundu & Gupta 2014). They derived a total energy of protons of $\sim 10^{60} \sim 10^{62}$ erg and the corresponding proton acceleration rate is $L_p = 10^{45} \sim 10^{47}$. Kundu & Gupta (2014) proposed that the X-ray fluxes of knot-A originate from the proton synchrotron radiation ($\delta = 1$) and obtained $L_p \sim 10^{43}$–10^{44} erg s^{-1} by assuming the jet age of 1.4×10^7 yr. Recently, Kusunose & Takahara (2018) used a photohadronic model to explain the X-ray emission of knot-A with the proton energy of 10^{61}–10^{62} erg. They estimated the proton power with $L_p \sim E_{p,total}/(3R/c) \sim 10^{50}$ erg s^{-1}, where $3R/c$ is the escape time of protons, and reported that the proton power can be lowered down to nearly Eddington power if the core photons are more beamed toward the X-ray knots than toward the line of sight. Chen (2018) also reported that the jet powers of some blazars may be super-Eddington. These results are consistent with ours. However, the super-Eddington issue could be relaxed by cutting down the low-energy protons, which are incapable of producing the observable photon flux, and might be avoided in the $\delta > 1$ case (see also Aharonian 2002).

As illustrated in Figure 3, the predicted fluxes in the GeV–TeV band by the SSC and IC/CMB processes of the two-electron populations are low; even in the $\delta > 1$ case (Figure 4), the predicted fluxes in the γ-ray band still cannot be detected by the available γ-ray detectors. As reported by Aharonian (2002), if the X-ray emission of large-scale jets is really dominated by the proton synchrotron, the most energetic protons with energies greater than 10^{19} eV may eventually escape the jet, which would result in different γ-ray emission characteristics depending on the magnetic field strength of the environment. Hence, the detection of γ-ray emission around the knots would

help exclude and constrain the radiation mechanism of the X-ray emission in large-scale jets.

4. Summary

Based on a comprehensively theoretical analysis of SED modeling, we suggested that the SEDs from the radio to X-ray bands of the large-scale jet knots in 3C 273 cannot be represented well with the synchrotron, SSC, and IC/CMB radiation of a single electron population when the Doppler boosting effect is either considered or not. We then considered two synchrotron radiation components to explain the broad-band SEDs of knots, from two independent electron populations (the leptonic model) or from an electron population plus a proton population (the hadronic model). Both models can represent the broadband SEDs of knots well. However, there is no observational evidence that different zones to accelerate two distinct electron populations. Particularly, the electrons with high energy that contribute X-ray emission have very short cooling times, thus it is hard to explain the observed X-ray morphologies of knots. In this respect, protons lose energy very slowly, thus their acceleration sites do not have to be within the emission sites. The proton synchrotron radiation model results in high jet powers, so-called "super-Eddington" jet powers. However, this issue might be avoided if these knots have relativistic motion toward the observer (see also Aharonian 2002). We also note that the knots may deviate from the equipartition condition if the X-ray emission is dominated by the synchrotron radiation of protons in the $\delta > 1$ case. The predicted γ-ray fluxes by the leptonic model through the IC process are very low, so the detection of γ-ray emission from knots in the future would help with examining models. Multiwavelength polarimetry observations with high resolution together, with the constraints on the magnetic field strength by Faraday rotation measurements, may shed light on the issue of particle acceleration and the emitting volume of particles. Further observations are required to confirm or rule out different models.

ORCID iDs

En-Wei Liang ⓘ https://orcid.org/0000-0002-7044-733X

References

Aab, A., Abreu, P., Aglietta, M., et al. 2018, ApJ, 868, 4
Abbasi, R. U., Abe, M., Abu-Zayyad, T., et al. 2017, APh, 86, 21
Abdo, A. A., Ackermann, M., Ajello, M., et al. 2010, Sci, 328, 725
Aharonian, F., Sun, X.-n., & Yang, R.-z. 2017, A&A, 603, A7
Aharonian, F. A. 2002, MNRAS, 332, 215
Arshakian, T. G., & Longair, M. S. 2004, MNRAS, 351, 727
Chen, L. 2018, ApJS, 235, 39
Conway, R. G., Garrington, S. T., Perley, R. A., et al. 1993, A&A, 267, 347
Croston, J. H., Hardcastle, M. J., Mingo, B., et al. 2011, ApJL, 734, L28
Dermer, C. D., & Schlickeiser, R. 1994, ApJS, 90, 945
Foreman-Mackey, D., Hogg, D. W., Lang, D., et al. 2013, PASP, 125, 306
Georganopoulos, M., & Kazanas, D. 2003, ApJL, 589, L5
Georganopoulos, M., Perlman, E. S., Kazanas, D., et al. 2006, ApJL, 653, L5
Gitti, M., O'Sullivan, E., Giacintucci, S., et al. 2010, ApJ, 714, 758

Gu, M., Cao, X., & Jiang, D. R. 2001, MNRAS, 327, 1111
Guo, S.-C., Zhang, H.-M., Zhang, J., et al. 2018, RAA, 18, 070
Hardcastle, M. J. 2006, MNRAS, 366, 1465
Harris, D. E., & Krawczynski, H. 2006, ARA&A, 44, 463
Hovatta, T., Valtaoja, E., Tornikoski, M., et al. 2009, A&A, 494, 527
Jester, S., Harris, D. E., Marshall, H. L., et al. 2006, ApJ, 648, 900
Jester, S., Meisenheimer, K., Martel, A. R., et al. 2007, MNRAS, 380, 828
Jester, S., Röser, H.-J., Meisenheimer, K., et al. 2005, A&A, 431, 477
Kataoka, J., & Stawarz, Ł. 2005, ApJ, 622, 797
Kraft, R. P., Nulsen, P. E. J., Birkinshaw, M., et al. 2007, ApJ, 665, 1129
Kundu, E., & Gupta, N. 2014, MNRAS, 444, L16
Kusunose, M., & Takahara, F. 2018, ApJ, 861, 152
Liodakis, I., Marchili, N., Angelakis, E., et al. 2017, MNRAS, 466, 4625
Lister, M. L., Cohen, M. H., Homan, D. C., et al. 2009, AJ, 138, 1874
Lister, M. L., Homan, D. C., Hovatta, T., et al. 2019, ApJ, 874, 43
McKeough, K., Siemiginowska, A., Cheung, C. C., et al. 2016, ApJ, 833, 123
Meisenheimer, K., Neumann, M., & Röser, H.-J. 1996, in Jets from Stars and
   Galactic Nuclei, ed. W. Kundt (Berlin: Springer), 230
Meyer, E. T., Georganopoulos, M., Sparks, W. B., et al. 2015, ApJ, 805, 154
Meyer, E. T., Iyer, A. R., Reddy, K., et al. 2019, ApJL, 883, L2
Meyer, E. T., Sparks, W. B., Georganopoulos, M., et al. 2016, ApJ, 818, 195
Mullin, L. M., & Hardcastle, M. J. 2009, MNRAS, 398, 1989
Neumann, M., Meisenheimer, K., & Roeser, H.-J. 1997, A&A, 326, 69
Nulsen, P. E. J., Hambrick, D. C., McNamara, B. R., et al. 2005, ApJL, 625, L9
Ostrowski, M. 1998, A&A, 335, 134

Perucho, M., Martí, J.-M., Quilis, V., et al. 2014, MNRAS, 445, 1462
Pierre Auger Collaboration, Abreu, P., Aglietta, M., et al. 2013, ApJL,
   762, L13
Rachen, J. P., & Biermann, P. L. 1993, A&A, 272, 161
Röser, H.-J., Meisenheimer, K., Neumann, M., et al. 2000, A&A, 360, 99
Sambruna, R. M., Donato, D., Tavecchio, F., et al. 2007, ApJ, 670, 74
Schmidt, M. 1963, Natur, 197, 1040
Schröder, F. G., AbuZayyad, T., Anchordoqui, L., et al. 2019, arXiv:1903.07713
Simionescu, A., Werner, N., Böhringer, H., et al. 2009, A&A, 493, 409
Stawarz, Ł., Cheung, C. C., Harris, D. E., & Ostrowski, M. 2007, ApJ,
   662, 213
Sun, X.-N., Yang, R.-Z., Rieger, F. M., et al. 2018, A&A, 612, A106
Tingay, S. J., Lenc, E., Brunetti, G., & Bondi, M. 2008, AJ, 136, 2473
Uchiyama, Y., Urry, C. M., Cheung, C. C., et al. 2006, ApJ, 648, 910
Wu, J., Ghisellini, G., Hodges-Kluck, E., et al. 2017, MNRAS, 468, 109
Zabalza, V. 2015, ICRC (The Hague), 34, 922
Zargaryan, D., Gasparyan, S., Baghmanyan, V., et al. 2017, A&A, 608, A37
Zhang, J., Bai, J.-M., Chen, L., et al. 2009, ApJ, 701, 423
Zhang, J., Bai, J. M., Chen, L., et al. 2010, ApJ, 710, 1017
Zhang, J., Du, S.-s., Guo, S.-C., et al. 2018a, ApJ, 858, 27
Zhang, J., Sun, X.-N., Liang, E.-W., et al. 2014, ApJ, 788, 104
Zhang, J., Xue, Z.-W., He, J.-J., Liang, E.-W., & Zhang, S.-N. 2015, ApJ,
   807, 51
Zhang, J., Zhang, H.-M., Yao, S., et al. 2018b, ApJ, 865, 100
Zirakashvili, V. N., & Aharonian, F. 2007, A&A, 465, 695